Applied Physics Letters

Phase engineering of monolayer transition-metal dichalcogenide through coupled electron doping and lattice deformation

Cite as: Appl. Phys. Lett. **107**, 191903 (2015); https://doi.org/10.1063/1.4934836
Submitted: 09 July 2015 . Accepted: 18 October 2015 . Published Online: 10 November 2015

Bin Ouyang, Guoqiang Lan, Yinsheng Guo, Zetian Mi, and Jun Song

Phase engineering of monolayer transition-metal dichalcogenide through coupled electron doping and lattice deformation

Bin Ouyang,[1] Guoqiang Lan,[1] Yinsheng Guo,[2] Zetian Mi,[3] and Jun Song[1,a)]
[1]*Department of Mining and Materials Engineering, McGill University, Montreal, Quebec H3A 0C5, Canada*
[2]*Department of Chemistry, Columbia University, New York, New York 10027, USA*
[3]*Department of Electrical and Computer Engineering, McGill University, Montreal, Quebec H3A 0E9, Canada*

(Received 9 July 2015; accepted 18 October 2015; published online 10 November 2015)

First-principles calculations were performed to investigate the phase stability and transition within four monolayer transition-metal dichalcogenide (TMD) systems, i.e., MX_2 (M = Mo or W and X = S or Se) under coupled electron doping and lattice deformation. With the lattice distortion and electron doping density treated as state variables, the energy surfaces of different phases were computed, and the diagrams of energetically preferred phases were constructed. These diagrams assess the competition between different phases and predict conditions of phase transitions for the TMDs considered. The interplay between lattice deformation and electron doping was identified as originating from the deformation induced band shifting and band bending. Based on our findings, a potential design strategy combining an efficient electrolytic gating and a lattice straining to achieve controllable phase engineering in TMD monolayers was demonstrated. © *2015 AIP Publishing LLC*.
[http://dx.doi.org/10.1063/1.4934836]

In the continuous research on two-dimensional (2D) materials, the development of atomically thin VI transition metal dichalcogenides (TMDs) brings new possibilities in the design of novel optical and electronic devices.[1–7] TMD consists of stacked 2D X-M-X layers bonded by weak interlayer van der Waals forces, where M is a transition metal while X is one of the three chalcogens, i.e., S, Se, and Te. With finite direct band gaps at visible or near infrared region and extraordinary absorption efficiencies, monolayer TMDs could serve as potential candidates in devices for solar energy[1,2,8,9] and illumination.[1,9,10] The sensitive responses of their electronic properties to deformation promise great potential for strain engineering, leading to a number of applications in bandgap engineering[4,6,12,29–31] and piezoelectronics,[11] among others. Furthermore, the strong spin-orbital coupling and the existence of multiple valleys at the conduction band minimum of TMDs also inspire applications in valleytronics.[6,7,12] One unique feature pertinent to the TMD family is the existence of multiple metastable 2D crystal phases.[13,14] For VI TMDs, the material can be either semiconducting or metallic depending on the crystal phase it assumes.[15–17] The polymorphism allows further enrichment and/or enhancement of the properties of TMDs,[14,15,18,19] and makes it possible to design chemically homogenous inherent TMD heterostructures.[14–16]

Till date, the electronic modification (e.g., intercalation)[19,20] and lattice deformation, e.g., external strain,[5,17,21] have been identified to be the two effective ways to induce phase transition in VI TMDs. Nonetheless, studies on the interplay between electronic modification and lattice deformation are largely absent. In this work, first-principles density functional theory (DFT) calculations were performed on four monolayer TMD systems, i.e., MX_2 (M = Mo, or W and X = S or Se). For each MX_2, the potential energy surfaces of the 2H, 1T, 1T′, and 1T″ phases were computed, and a diagram was constructed to assess the competition between different phases and predict conditions of phase transitions under coupled electron doping and in-plane lattice deformation. From the detailed analysis of electronic structures, the mechanistic origin underlying the interplay between the lattice deformation and electron doping was clarified. In the end, a potential design strategy combining the efficient electrolytic gating[22] and the lattice straining to achieve controllable phase engineering in TMD monolayer was demonstrated.

The first-principles DFT calculations employing the Perdew-Burke-Ernzerhof (PBE) functional and projector augmented-wave (PAW)[23] method were performed using the Vienna *ab initio* simulation package (VASP)[7] to examine physical and electronic properties of four phases, i.e., 2H, 1T, 1T′, and 1T″ of MX_2 (M = Mo or W and X = S or Se) monolayer. Below we use the notations 2H-MX_2 and 1T$^{\psi}$-MX_2 to denote TMD monolayers of 2H and 1T$^{\psi}$ (1T$^{\psi}$ = 1T, 1T′ or 1T″) phases. 2×2 supercells are constructed for the calculations of 2H-MX_2 and 1T-MX_2 while 1×2 and 1×1 supercells are constructed for the calculations of 1T′-MX_2 and 1T″-MX_2, respectively. The lattice configurations of those systems are illustrated in Fig. 1. From Fig. 1, we see that the 1T phase can be regarded as a structural transition from the 2H phase where the X atoms on one side of the M atoms are shifted to coincide (in the top view) with the centers of the hexagons formed by M atoms and other X atoms (cf. Fig. 1(a)). This transition results in a change of the symmetry from P63/mmc to P3. The 1T′ (cf. Fig. 1(b)) and 1T″ (cf. Fig. 1(c)) phases, on the other hand, are induced by further distortions (with reference to the 1T phase) of the M chain.[24] Considering the structural relation between different phases, in the context below, we will define a single lattice parameter a for simplicity, with $a = a_x$ for 2H and 1T phases, and $a = a_x/2$ for 1T′ and 1T″ phases.

a)Author to whom correspondence should be addressed. Electronic mail: jun.song2@mcgill.ca

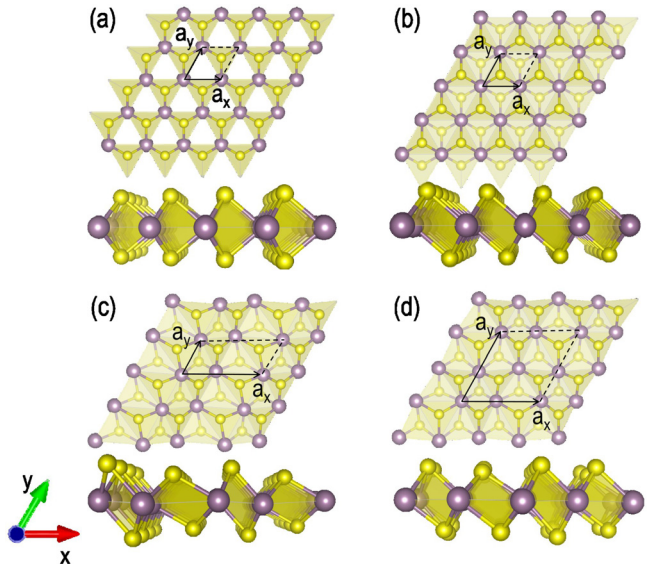

FIG. 1. Atomic configurations of different TMD phases: (a) 2H, (b) 1T, (c) 1T′, and (d) 1T″ phases. The black quadrilateral illustrated the unit cell, with the large purple and small yellow spheres indicating metal and chalcogen atoms, respectively.

In each calculation, a $7 \times 7 \times 1$ k-point grid and an energy cutoff of 400 eV were adopted. Benchmark calculations using more k-points and larger energy cutoff values have been performed, showing an energy difference smaller than 0.02 eV. The vacuum space between the monolayer and its neighboring periodic image is set as 20 Å in thickness (along the direction perpendicular to the monolayer) to eliminate image interactions.

From DFT calculations, the ground states of different phases for the four TMD systems were obtained. One thing to note is that for all these systems, the 1T phase was found to exhibit much higher energy than other phases for the ranges of strain and electron doping density (see below) examined,[25] which essentially renders it thermodynamically unstable. The instability of the 1T phase is also evidenced by the appearance of imaginary frequencies in the phonon dispersion spectrum.[25] As a consequence, below we limit our discussion to 2H, 1T′, and 1T″ phases.

Starting from those ground states, the effects of deformation (i.e., biaxial straining) and electron doping on the energetics were examined. Here, we denote E as the total energy per primitive cell and q as the electron doping density, i.e., the number of electrons injected per primitive cell (the primitive cell is defined with reference to the 2H phase). With the area of the primitive cell being 8.8×10^{-20} m^2, one electron injected into a primitive cell will produce an electron doping density of $q_0 = 1.14 \times 10^{15}\,\mathrm{cm}^{-2}$. In the following context, we represent q in the unit of q_0 for simplicity. Figs. 2(a)–2(d) show the evolution of E of different phases in each TMD system as the lattice constant varies for three representative q values (i.e., $q = 0$, 0.4 q_0, and 0.8 q_0). In particular, we introduce a lattice distortion ratio $\Delta a/a_0 = (a - a_0)/a_0$ to describe the deformation, where a_0 denotes the ground state lattice constant of the intrinsic 2H phase (the values of a_0 for other phases are listed in Table SI).

Several interesting observations can be drawn from Figs. 2(a)–2(d). First, we note that for a particular q, the

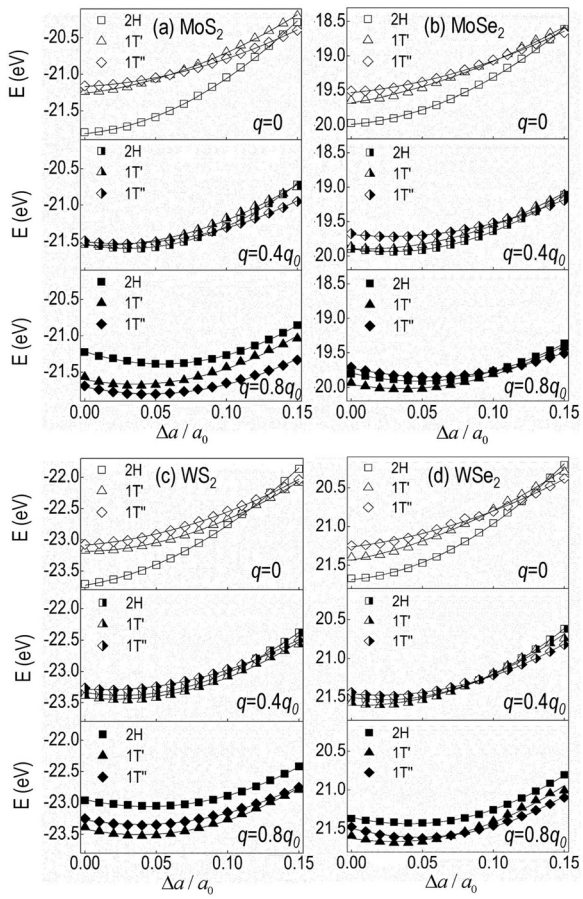

FIG. 2. The evolutions of energy E vs. lattice deformation $\Delta a/a_0$ at three different electron doping densities, $q = 0$, $0.4q_0$, and $0.8q_0$ ($q_0 = 1.14 \times 10^{15}\,\mathrm{cm}^{-2}$) for (a) MoS_2, (b) $MoSe_2$, (c) WS_2, and (d) WSe_2 systems.

energy E exhibits a quadratic dependence on $\Delta a/a_0$. Second, we see that the equilibrium lattice constant, i.e., the lattice constant at which E is minimized, varies as the q changes. Third, we see that particularly for the 2H phase, overall the system energy is considerably elevated with respect to the other two phases accompanying the injection of electrons. To quantitatively analyze the above observations, we consider a MX_2 phase of an electron doping density q and a lattice constant a. The energy E of this system includes a strain energy component E_s that can be expressed as (assuming linear elasticity)

$$E_s = \frac{1}{2} k \varepsilon^2, \tag{1}$$

where k is the effective stiffness[26] and ε is the strain, being $\varepsilon = (a - a_q)/a_q$. Here, a_q denotes the equilibrium lattice constant of the reference 2H-MX_2 primitive cell (of an electron doping density q). With Eq. (1), we have

$$\begin{aligned} E &= E_0^q + E_s = E_0^q + \frac{1}{2} k \varepsilon^2 \\ &= E_0^q + \frac{1}{2} k \left(\frac{a - a_q}{a_q} \right)^2 = E_0^q + \frac{1}{2} \frac{k a_0^2}{a_q^2} \left(\frac{\Delta a}{a_0} \right)^2, \end{aligned} \tag{2}$$

where E_0^q denotes the corresponding value of E at $a = a_q$ (i.e., the ground state energy) while the term ka_0^2/a_q^2

corresponds to the curvature of the E vs. $\Delta a/a_0$ curve at at $a = a_q$. For Eq. (2), we can see the observed quadratic dependence of E vs. $\Delta a/a_0$ in Fig. 2 directly derives from the quadratic nature of the strain energy E_s.

The evolutions of a_q, k, and E_0^q vs. q are shown in Figs. 3(a)–3(d). We can see that the equilibrium lattice constant (i.e., a_q) always monotonically increases as q increases, suggesting that electron doping induces lattice expansion. The effective stiffness k, meanwhile, exhibits distinct trends for 2H and 1T′/1T″ phases. Specifically, we note that for the 1T′/1T″ phases k either remains largely unchanged or slightly increases (e.g., MoS_2) while for the 2H phase k shows sizable decrease (albeit ignorable increment in k in the cases of MoS_2 and WS_2 at $q < 0.1\ q_0$) as q increases. This indicates that the 2H phase is greatly softened accompanying the injection of electrons. Furthermore, when it comes to E_0^q, we see that for the 2H phase, E_0^q generally increases as electrons are introduced, while the opposite trend is observed for the 1T′ and 1T″ phases. Particularly, we note that the 2H phase has the lowest E_0^q at small q values but exhibits the largest E_0^q at high values of q. This implies that the injection of electrons can facilitate transition from 2H to 1T′/1T″.

The afore-mentioned results demonstrate that the competition between different MX_2 phases can be tuned by strain and electron doping. With $\Delta a/a_0$ and q treated as state variables, the energy surfaces of different phases were computed,[25] and the diagrams of energetically preferred phases were constructed for each TMD system, shown in Fig. 4.

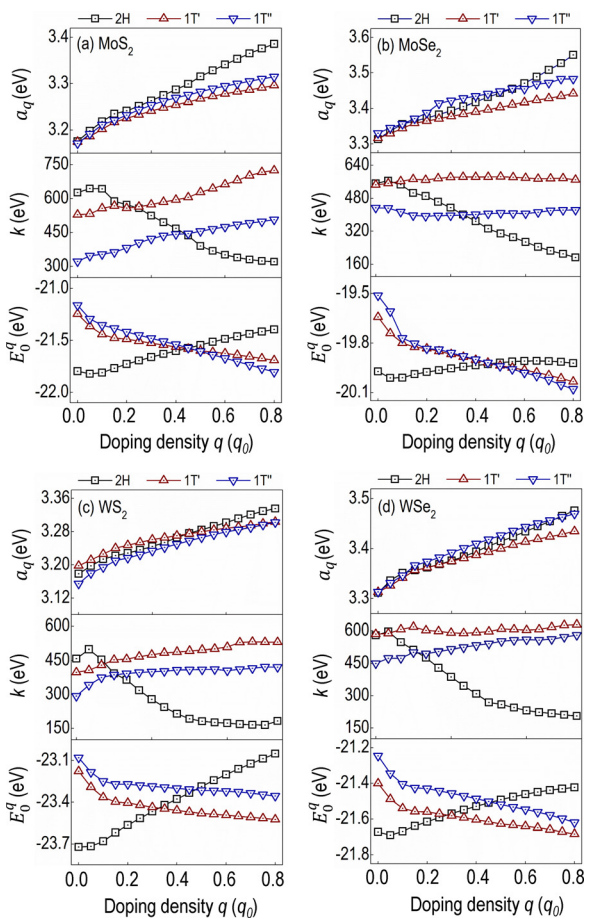

FIG. 3. The evolutions of a_q, k, and E_0^q as functions of the doping density q for (a) MoS_2, (b) $MoSe_2$, (c) WS_2, and (d) WSe_2 systems.

Fig. 4 provides direct predictions of transitions between 2H, 1T′, and 1T″ phases. It also provides valuable information on the coupling between electron doping and lattice distortion. For simplicity, in our discussion below, we select WSe_2 as a representation.[27] The effects of electron doping on 2H → 1T′/1T″ transition largely derives from the fact that the 2H phase is a semiconductor,[28] while 1T′ and 1T″ are nearly metallic. On the other hand, lattice deformation induces band shifting and band bending,[4,29,30] thus necessarily meshes with the effects of electron doping. Fig. 5(a) presents the energy (E) difference between 2H-WSe_2 and 1T′/1T″-WSe_2 as q varies at different $\Delta a/a_0$ values. We see that those curves in Fig. 5(a) exhibit a general increasing trend as q increases. However, the rate of increment decreases as $\Delta a/a_0$ rises, being particularly pronounced at the larger $\Delta a/a_0$ values (e.g., $\Delta a/a_0 = 0.12$). This observation can be directly traced to the influence of lattice distortion on the energy gaps, i.e., Γ-K, K-K, and band gaps, of the 2H phase, shown in Fig. 5(b). We see that these energy gaps decrease as $\Delta a/a_0$ increases. Particularly, the band gap becomes zero when $\Delta a/a_0$ goes beyond 0.11. Within the zero band gap regime, 2H-WSe_2 becomes metallic, same as 1T′/1T″-WSe_2,[31] consequently rendering the energy difference, i.e., $E(2H) - E(1T'/1T'')$, insensitive to electron doping (cf. Fig. 4(a), where curves are nearly flat at $\Delta a/a_0 = 0.12$).

Another observation from Fig. 4 is that with lattice straining, the 2H-1T″ transition can occur at a low level of electron doping. For instance, in the case of WSe_2, with $\Delta a/a_0$ being in the range of 0.94 to 0.15, the 2H-1T″ transition can be induced by a rather small electron doping density of $q = 0.1\ q_0 = 1.14 \times 10^{14}\,\mathrm{cm}^{-2}$ (see Fig. 5(c)). One way to realize electron doping experimentally is electron gating, the capacity of which was demonstrated in the study by Efetov and Kim[22] where an electron doping density of $4 \times 10^{14}\,\mathrm{cm}^{-2}$ was achieved. Hence, we propose a possible design, illustrated by the schematic in Fig. 5(c), which consists of a pre-strained WSe_2 monolayer and a simple gate switch. In this design, by controlling the degree of lattice deformation (e.g., through

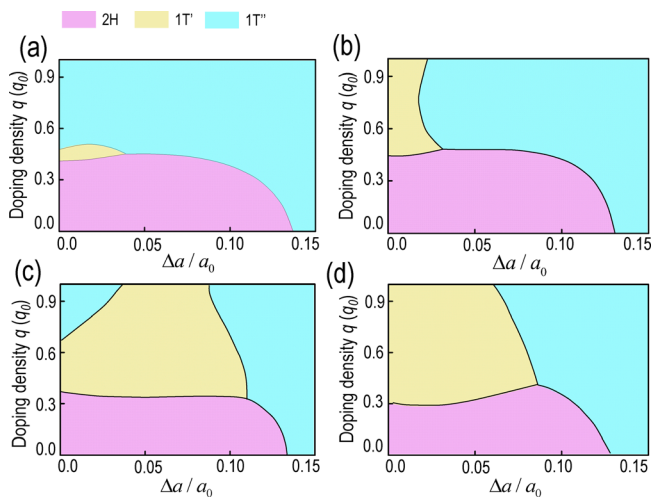

FIG. 4. Diagrams of energetically preferred phases as the lattice deformation $\Delta a/a_0$ and electron doping density q vary for (a) MoS_2, (b) $MoSe_2$, (c) WS_2, and (d) WSe_2. The domains corresponding to 2H, 1T′, and 1T″ in each diagram are colored purple, yellow, and blue, respectively.

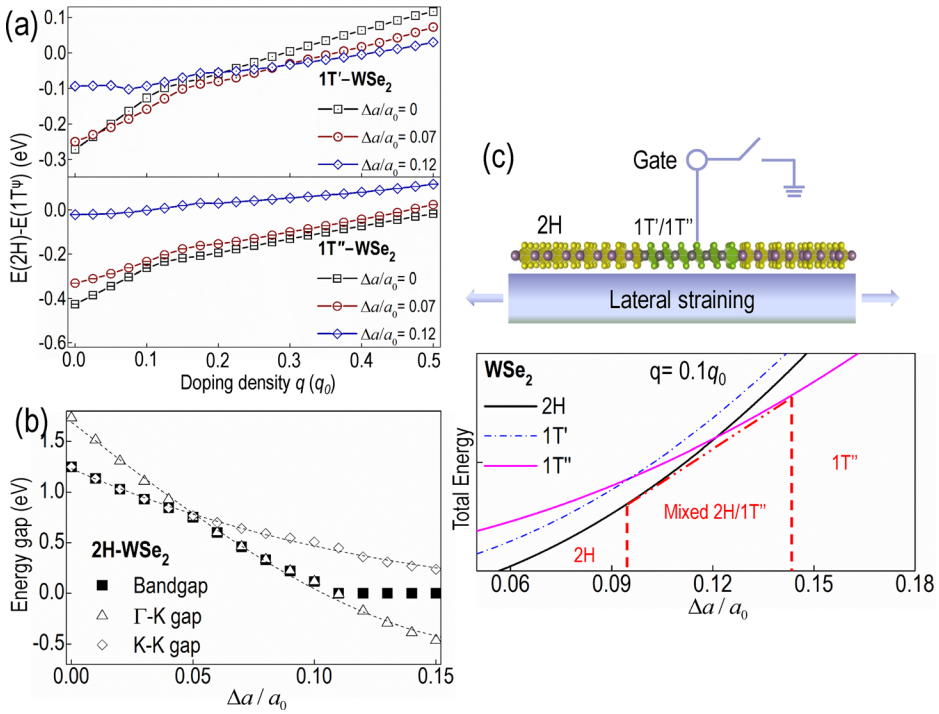

FIG. 5. (a) Energy differences $E(2H) - E(1T^{\psi})$ as functions of the electron doping density q at different levels of lattice deformation (i.e., $\Delta a/a_0$) for WSe_2, where $E(1T^{\psi})$ with $1T^{\psi} = 1T'$ or $1T''$ denotes the energy of the $1T'$ or $1T''$ phase respectively while $E(2H)$ denotes the energy of the 2H phase. (b) The variation in energy gaps, i.e., bandgap, Γ-K gap and K-K gap, as $\Delta a/a_0$ varies. (c) Schematic illustration of a possible phase transition route through substrate-induced lattice straining and gating (i.e., the switch at a gate to adjust electron doping), the inset below the schematic shows the energy profiles of 2H, $1T'$, and $1T''$ phases as functions of the lattice deformation at an electron doping density of $q = 0.1q_0$. The phases expected in different regimes of lattice deformation are indicated.

substrate,[4,21,29,32] intercalation,[15,16,33] or other means), controllable phase engineering can be achieved. This promises insights towards designing smart and tunable TMD based devices.

To conclude, we have performed first-principles calculations to investigate the phase stability and transition within four types of monolayer TMD systems. The energetics of 2H, 1T, $1T'$, and $1T''$ phases under coupled in-plane lattice distortion and electron doping were examined. For all TMD systems examined, a competition exists between 2H, $1T'$, and $1T''$ phases as the levels of lattice distortion and electron doping vary, while the 1T phase is expected to be unstable due to its high energy. With the lattice distortion and electron doping density treated as state variables, the energy surfaces of different phases were computed for those TMD systems considered, and the diagrams of energetically preferred phases were constructed. These diagrams directly outline phase boundaries between 2H, $1T'$, and $1T''$ phases. They also provide essential information on the interplay between electron doping and lattice deformation, which was identified to be originated from the deformation induced band shifting and band bending. The coupling between electron doping and lattice deformation promises interesting implications in the design of TMD based devices, and one possible route combining electron gating and lattice straining to achieve controllable phase engineering in MX_2 monolayer was demonstrated.

The authors would like to thank the financial support from McConnell Memorial Fellowship in Engineering, McGill Engineering Doctorate Award, and NSERC Discovery Grant (Grant No. RGPIN 418469-2012). The authors also like to acknowledge Supercomputer Consortium Laval UQAM McGill and Eastern Quebec for providing computing power.

[1]O. Lopez-Sanchez, E. A. Llado, V. Koman, A. Fontcuberta i Morral, A. Radenovic, and A. Kis, ACS Nano **8**(3), 3042 (2014).
[2]M. Bernardi, M. Palummo, and J. C. Grossman, Nano Lett. **13**(8), 3664 (2013); Ji. Feng, X. Qian, C.-W. Huang, and Ju. Li, Nat. Photonics **6**(12), 866 (2012).
[3]M. Buscema, M. Barkelid, V. Zwiller, H. S. J. van der Zant, G. A. Steele, and A. Castellanos-Gomez, Nano Lett. **13**(2), 358 (2013); S. Huang, Xi. Ling, L. Liang, J. Kong, H. Terrones, V. Meunier, and M. S. Dresselhaus, *ibid.* **14**(10), 5500 (2014); A. Splendiani, L. Sun, Y. Zhang, T. Li, J. Kim, C.-Y. Chim, G. Galli, and F. Wang, *ibid.* **10**(4), 1271 (2010); K. F. Mak, K. He, C. Lee, G. H. Lee, J. Hone, T. F. Heinz, and J. Shan, Nat. Mater. **12**(3), 207 (2013); X. Hong, J. Kim, Su.-F. Shi, Yu. Zhang, C. Jin, Y. Sun, S. Tongay, J. Wu, Y. Zhang, and F. Wang, Nat. Nanotechnol. **9**(9), 682 (2014); F. H. L. Koppens, T. Mueller, Ph. Avouris, A. C. Ferrari, M. S. Vitiello, and M. Polini, *ibid.* **9**(10), 780 (2014).
[4]H. J. Conley, B. Wang, J. I. Ziegler, R. F. Haglund, S. T. Pantelides, and K. I. Bolotin, Nano Lett. **13**(8), 3626 (2013).
[5]A. P. Nayak, T. Pandey, D. Voiry, J. Liu, S. T. Moran, A. Sharma, C. Tan, C.-H. Chen, L.-J. Li, M. Chhowalla, J.-Fu. Lin, A. K. Singh, and D. Akinwande, Nano Lett. **15**(1), 346 (2015).
[6]K. F. Mak, K. He, J. Shan, and T. F. Heinz, Nat. Nanotechnol. **7**(8), 494 (2012); A. Chernikov, T. C. Berkelbach, H. M. Hill, A. Rigosi, Y. Li, O. B. Aslan, D. R. Reichman, M. S. Hybertsen, and T. F. Heinz, Phys. Rev. Lett. **113**(7), 076802 (2014); Y. Li, J. Ludwig, T. Low, A. Chernikov, Xu. Cui, G. Arefe, Y. D. Kim, A. M. van der Zande, A. Rigosi, H. M. Hill, S. H. Kim, J. Hone, Z. Li, D. Smirnov, and T. F. Heinz, *ibid.* **113**(26), 266804 (2014); D. MacNeill, C. Heikes, K. Fai Mak, Z. Anderson, A. Kormányos, V. Zólyomi, J. Park, and D. C. Ralph, *ibid.* **114**(3), 037401 (2015).
[7]K. He, N. Kumar, L. Zhao, Z. Wang, K. F. Mak, H. Zhao, and J. Shan, Phys. Rev. Lett. **113**(2), 026803 (2014).
[8]M. Wu, X. Qian, and Ju. Li, Nano Lett. **14**(9), 5350 (2014); M.-L. Tsai, S.-H. Su, J.-K. Chang, D.-S. Tsai, C.-H. Chen, C.-I. Wu, L.-J. Li, L.-J. Chen, and Jr.-H. He, ACS Nano **8**(8), 8317 (2014); Y. J. Zhang, J. T. Ye, Y. Yomogida, T. Takenobu, and Y. Iwasa, Nano Lett. **13**(7), 3023 (2013).
[9]C.-Ho. Lee, G.-H. Lee, A. M. van der Zande, W. Chen, Y. Li, M. Han, Xu. Cui, G. Arefe, C. Nuckolls, T. F. Heinz, J. Guo, J. Hone, and P. Kim, Nat. Nanotechnol. **9**(9), 676 (2014).
[10]S. Tongay, J. Suh, C. Ataca, W. Fan, A. Luce, J. S. Kang, J. Liu, C. Ko, R. Raghunathanan, J. Zhou, F. Ogletree, J. Li, J. C. Grossman, and J. Wu, Sci. Rep. **3**, 2657 (2013); K. Roy, M. Padmanabhan, S. Goswami, T. P. Sai, G. Ramalingam, S. Raghavan, and A. Ghosh, Nat. Nanotechnol. **8**(11), 826 (2013); R. S. Sundaram, M. Engel, A. Lombardo, R. Krupke, A. C. Ferrari, Ph. Avouris, and M. Steiner, Nano Lett. **13**(4), 1416 (2013).

[11]M.-Y. Tsai, A. Tarasov, Z. R. Hesabi, H. Taghinejad, P. M. Campbell, C. A. Joiner, A. Adibi, and E. M. Vogel, ACS Appl. Mater. Interfaces **7**(23), 12850 (2015); T. Wu and H. Zhang, Angew. Chem. **127**(15), 4508 (2015); E. J. Reed, Nat. Nanotechnol. **10**(2), 106 (2015); H. Zhu, Y. Wang, J. Xiao, M. Liu, S. Xiong, Zi. J. Wong, Z. Ye, Yu. Ye, X. Yin, and X. Zhang, *ibid.* **10**(2), 151 (2015); W. Wu, L. Wang, Y. Li, F. Zhang, L. Lin, S. Niu, D. Chenet, X. Zhang, Y. Hao, T. F. Heinz, J. Hone, and Z. L. Wang, Nature **514**(7523), 470 (2014).
[12]A. Ramasubramaniam, Phys. Rev. B **86**(11), 115409 (2012); Di. Xiao, G.-B. Liu, W. Feng, X. Xu, and W. Yao, Phys. Rev. Lett. **108**(19), 196802 (2012); K. F. Mak, K. L. McGill, J. Park, and P. L. McEuen, Science **344**(6191), 1489 (2014).
[13]J. A. Wilson and A. D. Yoffe, Adv. Phys. **18**(73), 193 (1969); R. H. Friend and A. D. Yoffe, *ibid.* **36**(1), 1 (1987).
[14]G. Eda, T. Fujita, H. Yamaguchi, D. Voiry, M. Chen, and M. Chhowalla, ACS Nano **6**(8), 7311 (2012).
[15]D. Voiry, A. Goswami, R. Kappera, C. de Carvalho Castro e Silva, D. Kaplan, T. Fujita, M. Chen, T. Asefa, and M. Chhowalla, Nat. Chem. **7**(1), 45 (2015).
[16]R. Kappera, D. Voiry, S. E. Yalcin, B. Branch, G. Gupta, A. D. Mohite, and M. Chhowalla, Nat. Mater. **13**(12), 1128 (2014).
[17]A. P. Nayak, S. Bhattacharyya, J. Zhu, J. Liu, X. Wu, T. Pandey, C. Jin, A. K. Singh, D. Akinwande, and J.-Fu. Lin, Nat. Commun. **5**, 3731 (2014).
[18]H. Wang, Z. Lu, S. Xu, D. Kong, J. J. Cha, G. Zheng, Po.-C. Hsu, K. Yan, D. Bradshaw, F. B. Prinz, and Yi. Cui, Proc. Natl. Acad. Sci. **110**(49), 19701 (2013); M. A. Lukowski, A. S. Daniel, F. Meng, A. Forticaux, L. Li, and S. Jin, J. Am. Chem. Soc. **135**(28), 10274 (2013); Y. Guo, D. Sun, B. Ouyang, A. Raja, J. Song, T. F. Heinz, and L. E. Brus, Nano Lett. **15**(8), 5081 (2015).
[19]L. Wang, Z. Xu, W. Wang, and X. Bai, J. Am. Chem. Soc. **136**(18), 6693 (2014).
[20]M. Kan, J. Y. Wang, X. W. Li, S. H. Zhang, Y. W. Li, Y. Kawazoe, Q. Sun, and P. Jena, J. Phys. Chem. C **118**(3), 1515 (2014); A. N. Enyashin, L. Yadgarov, L. Houben, I. Popov, M. Weidenbach, R. Tenne, M. Bar-Sadan, and G. Seifert, *ibid.* **115**(50), 24586 (2011).
[21]K.-A. N. Duerloo, Y. Li, and E. J. Reed, Nat. Commun. **5**, 4214 (2014).
[22]D. K. Efetov and P. Kim, Phys. Rev. Lett. **105**(25), 256805 (2010); B. Chakraborty, A. Bera, D. V. S. Muthu, S. Bhowmick, U. V. Waghmare, and A. K. Sood, Phys. Rev. B **85**(16), 161403 (2012); G. P. Siddons, D. Merchin, Ju. H. Back, J. K. Jeong, and M. Shim, Nano Lett. **4**(5), 927 (2004); L. Ming-Wei, L. Lezhang, L. Qing, T. Xuebin, S. D. Kulwinder, Z. Peng, M. N. Vaman, C. M. Ming-Cheng, and Z. Zhixian, J. Phys. D: Appl. Phys. **45**(34), 345102 (2012).
[23]P. Hohenberg and W. Kohn, Phys. Rev. **136**(3B), B864 (1964); W. Kohn and L. J. Sham, *ibid.* **140**(4A), A1133 (1965); P. E. Blöchl, Phys. Rev. B **50**(24), 17953 (1994); G. Kresse and J. Furthmüller, *ibid.* **54**(16), 11169 (1996); J. P. Perdew, K. Burke, and M. Ernzerhof, Phys. Rev. Lett. **77**(18), 3865 (1996).
[24]E. Benavente, M. A. Santa Ana, F. Mendizábal, and G. González, Coord. Chem. Rev. **224**(1–2), 87 (2002).
[25]See supplementary material at http://dx.doi.org/10.1063/1.4934836 for additional information on 1T-MX_2 and on the construction of the 2D diagrams in Fig. 4.
[26]Strictly speaking, k is the product of the actual stiffness and volume of the primitive cell.
[27]Note: Similar findings are obtained for other TMD systems as well.
[28]Note: It is worth noting that under large strains the 2H phase becomes metallic.
[29]A. Castellanos-Gomez, R. Roldán, E. Cappelluti, M. Buscema, F. Guinea, H. S. J. van der Zant, and G. A. Steele, Nano Lett. **13**(11), 5361 (2013).
[30]N. Lu, H. Guo, L. Li, J. Dai, Lu. Wang, W.-N. Mei, X. Wu, and X. C. Zeng, Nanoscale **6**(5), 2879 (2014).
[31]Notes: Meanwhile, 1T′ and 1T″ phases remain metallic, regardless of the lattice distortion.
[32]S. Bertolazzi, J. Brivio, and A. Kis, ACS Nano **5**(12), 9703 (2011).
[33]R. Kappera, D. Voiry, S. E. Yalcin, W. Jen, M. Acerce, S. Torrel, B. Branch, S. Lei, W. Chen, S. Najmaei, J. Lou, P. M. Ajayan, G. Gupta, A. D. Mohite, and M. Chhowalla, APL Mater. **2**(9), 092516 (2014).